PHYSICAL REVIEW B VOLUME 31, NUMBER 5 1 MARCH 1985

Magnetic excitations in chromium. II

B. H. Grier* and G. Shirane
Physics Department, Brookhaven National Laboratory, Upton, New York 11973

S. A. Werner†
Center for Materials Science, National Bureau of Standards, Washington, D.C., 20234
(Received 2 August 1984)

Neutron scattering measurements on pure chromium metal have been performed under various conditions of experimental resolution, energy transfer, temperature, and magnetic field. The temperature and energy dependence of the commensurate-diffuse scattering surrounding the (0,0,1) point in reciprocal space has been followed from the spin-flip temperature ($T_{sf}=122$ K) to temperatures as high as 700 K, well above the Néel point ($T_N=312$ K). Magnetic correlations extending over 11 bcc unit cells persist to these high temperatures. The spectral width of the magnetic scattering is found to increase rapidly with temperature above T_N. The importance of the commensurate-diffuse modes of excitation in the disappearance of the long-range-ordered spin-density-wave (SDW) state at T_N is discussed. The magnetic field dependence of the excitations in the transversely polarized SDW phase has been investigated and found to be absent. Evidence is also presented for the absence of a spin-wave energy gap greater than 50 μeV. We have placed the scattering in the paramagnetic phase on an absolute scale by normalizing to the integrated intensities of selected phonons, and have estimated an effective magnetic moment per atom.

I. INTRODUCTION

Experimental studies of chromium metal have continued to provide an array of surprises since the discovery of the incommensurate, sinusoidally modulated nature of the antiferromagnetism occurring in this material more than 20 years ago.[1,2] This unique, itinerant-electron magnetic state is due to the presence of an Overhauser spin-density wave (SDW).[3] As first pointed out by Lomer[4] this state occurs in chromium because of the nearly perfect nesting of portions of the "jack-shaped" electron Fermi surface surrounding the Γ point (0,0,0) in reciprocal space with flat portions of the octahedral-shaped hole surface surrounding the H point (1,0,0).[5] Two-band theoretical models based on those ideas successfully account for many of the observed magnetic properties of chromium and its dilute alloys, including the magnitude and variation of the wave vector **Q**, the amplitude of the SDW, and the ordering temperature.[6]

Until recently, relatively little was known experimentally about the elementary excitations of the SDW in pure chromium.[7–12] Theories of the long-wavelength spin waves have been developed based on various simplifying two-band models by Fedders and Martin,[13] by Liu,[14] and by Sato and Maki.[15] These theories predict the occurrence of very-high-velocity spin waves, comparable to the Fermi velocity. The predictions do not seem to depend strongly upon the extent of commensurability of the SDW. Neutron inelastic scattering measurements on commensurate *Cr*Mn alloys[16,17] give a spin-wave velocity of about 1.5×10^7 cm/sec, in rough agreement with theoretical predictions. Wolfram and Ellialtioglu[18] have investigated the magnetic excitations of a one-dimensional, sinusoidally modulated spin structure using an equation-of-motion method and a Hamiltonian which explicitly builds in the observed SDW ground state. Certain aspects of the magnetic scattering cross section of Cr observed in recent experiments can be accounted for by this calculation, while others cannot. Generally speaking, the current theories are not consistent in their predictions, and do not even suggest some of the most salient features of the neutron scattering experiments carried out during the last several years. It is apparent that an understanding of the magnetic excitations in pure chromium presents an important theoretical challenge in itinerant-electron magnetism. This paper represents a continuation of our inelastic neutron scattering work described in Ref. 9, with special emphasis on the evolution of the magnetic scattering from the low-temperature SDW phases to far into the paramagnetic phase.

II. MAGNETIC PROPERTIES OF CHROMIUM

In order that the experiments described in this paper can be more easily understood and properly motivated, we begin here by giving a brief summary of the main features of our earlier results[9] along with certain aspects of the magnetic properties of Cr obtained from other measurements.

There are three magnetic phases of Cr. At temperatures below the spin-flip temperature ($T_{sf}=122$ K) the fundamental SDW is longitudinally polarized. Above T_{sf} the SDW is transversely polarized up to the first-order transition at the Néel point ($T_N=312$ K).[19] As a result of the cubic symmetry of paramagnetic Cr, three types of domains develop below T_N with the **Q** vector of the SDW along any one of the three [100]-type directions in the crystal giving rise to equivalent sets of magnetic satellites.

A single-**Q** state is produced by cooling the crystal through the Néel point in the presence of a large magnetic field directed along a [100] axis.[20] This procedure results in a crystal consisting of one type of **Q** domain with the modulation direction along the applied field. The crystal will remain in this state after the field is reduced to zero, so long as the temperature is not raised above T_N. The reciprocal lattice shown in Fig. 1 is for a "field-cooled" crystal with the single-**Q** direction along [001]. The magnitude of Q is $0.9515a^*$ ($a^*=2\pi/a$, where a is the bcc lattice parameter) at low temperatures and increases slightly with temperature. The ability to create this microscopic single-**Q** state in a large crystal considerably simplifies inelastic scattering experiments on pure Cr.

In Fig. 2 we reproduce the results[9] of a constant-energy scan along the [001] direction, across the satellite positions near the (0,0,1) point in reciprocal space at $T=200$ K. As expected from elementary theoretical considerations, strong scattering is observed near the satellite Bragg points, from which high-velocity spin-wave dispersion surfaces originate. Because the dimensions of the dispersion surfaces in momentum space are much smaller than the resolution ellipsoid, single peaks are observed at $0.95a^*$ and at $1.05a^*$. In addition to the spin-wave scattering, there is an additional feature centered at the commensurate point (0,0,1). We refer to this feature as the "commensurate-diffuse" scattering. It persists throughout the transversely polarized phase, increasing rapidly as the temperature approaches T_N. We have now studied this temperature dependence in some detail as discussed later. This commensurate-diffuse scattering also increases rapidly with decreasing energy transfer, showing a peak at about 4 meV, as seen from the constant-**Q** scan shown in the inset in Fig. 2. These components of the magnetic scattering cross section were unexpected from theoretical considerations and were, in fact, first observed in the earlier measurements of Mikke and Jankowski.[8] Recently, Burke *et al.*[12] have observed a splitting of this commensurate-diffuse scattering in the region between 4 to 8 meV, suggesting that it may somehow be connected with the longitudinal phonon modes. We will discuss this possibility in Sec. IV.

Previous neutron-diffraction experiments[20–22] have shown that the polarization of the SDW in the transverse phase can be easily rotated in the **x**-**y** plane (normal to **Q**)

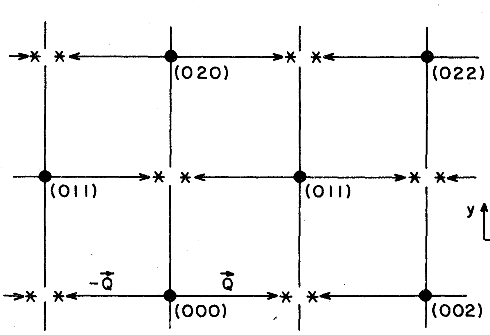

FIG. 1. The (100) reciprocal-lattice plane of antiferromagnetic chromium in a single-**Q** state. The solid circles are bcc nuclear Bragg reflections. The stars are magnetic satellite points.

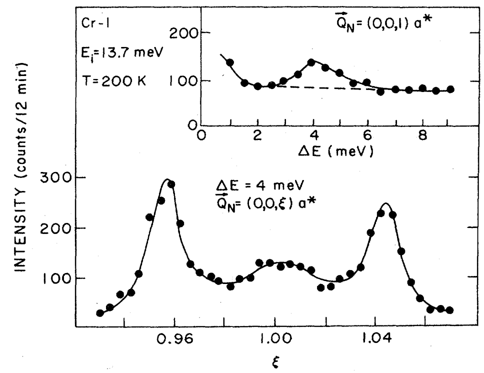

FIG. 2. This figure is a reproduction of data given in Ref. 9. The constant-energy scan at $\Delta E=4$ meV shows two spin-wave peaks centered at wave vectors corresponding to the magnetic satellite points near (0,0,1) in Fig. 1, and the commensurate-diffuse scattering centered at (0,0,1). A constant-**Q** scan at a neutron scattering vector $\mathbf{Q}_N=(0,0,1)a^*$ is shown in the inset. (To avoid confusion, we use a subscript N on the neutron scattering vector $\mathbf{Q}_N$ to distinguish it from the SDW wave vectors **Q**.)

by applying a magnetic field **H** normal to **Q**. The spin direction tends to align perpendicular to both **Q** and **H**, as is expected in any antiferromagnet where the dc perpendicular susceptibility $\chi_\perp$ is larger than the parallel susceptibility $\chi_{\parallel}$. Since $\Delta\chi$ ($=\chi_\perp-\chi_{\parallel}$) is quite small for Cr, and since a rather modest magnetic field of order 20 kOe is sufficient to rotate nearly all of the spins (in the best crystals), the magnetic energies per atom involved in this rotation process are very small. It was found that the spin directions were confined to the **x**-**y** plane, and that this reorientation process was strongly temperature dependent, being more difficult to saturate at higher temperatures. From these observations, one would conclude that there are low energy transverse (to **Q**) fluctuations of the polarization of the SDW. We initially conjectured that the commensurate-diffuse scattering might be related to these fluctuations. On the basis of these ideas we have carried out inelastic neutron scattering experiments on Cr in the presence of magnetic fields up to 60 kOe, as discussed in the next section.

Because of the incommensurate nature of the SDW in pure Cr, one has the opportunity to directly measure the polarization of the spin-wave excitations with unpolarized neutrons by observing the ratio of the intensities of the spin waves at $(0,0,1-\delta)$ and at $(0,1,\delta)$. Due to the large anisotropy confining the polarization of the static SDW to the **x**-**y** plane in the transverse phase, one might expect that the spin-wave fluctuations would also be anisotropic. Our original observations tended to support this expectation. However, we have now found that this conclusion was obviated by anisotropic sample container transmission effects, and that the spin-wave fluctuations are isotropic above about 4 meV. Recent experiments at Grenoble[12] have pursued this question in somewhat more detail. It is found that the expected anisotropy does in fact occur for the lower-energy spin waves.

The fluctuations responsible for the disappearance of the ordered SDW state at the Néel point have been of long-standing interest, and have motivated many of the recent neutron experiments on Cr, including those reported here. All of the current theories assume that the average amplitude of the local spin density goes to zero at T_N in a self-consistent way as the energy gap created at the Fermi surface by the SDW vanishes. This assumption has been supported by the reported absence of any significant paramagnetic scattering of neutrons above T_N and the smallness of the anomaly in the heat capacity at T_N.[23,24] The effects of residual strain on the character of the transition at the Néel point, and even the temperature at which it occurs, have made a detailed study of this question more difficult.[19,25] For this reason we have carried out experiments on several different crystals prepared by vapor deposition and by the strain-and-anneal technique. Results of our recent experiments, given in Sec. III, near and far above T_N reveal that there is significant magnetic scattering in the paramagnetic phase, and that the disappearance of the long-range-ordered SDW state is intimately connected with the commensurate-diffuse excitations.

III. EXPERIMENTAL RESULTS

The experiments discussed in this paper were carried out on three different single crystals of high-purity chromium, including the same two crystals used in the work on Ref. 9. Most of the work below the Néel point ($T_N=312$ K) was performed on the sample Cr-1. This crystal was grown from the vapor in the decomposition of chromium iodide; it has a mosaic width of less than 5′ and is approximately 0.5 cm^3. This crystal was studied after being transformed to a single-**Q** state by cooling through T_N in a magnetic field of 60 kOe directed along the [001] bcc axis. Most of the measurements near and above T_N were performed on Cr-2; it is a crystal of about 2 cm^3, roughly cylindrical in shape grown by strain and anneal with a mosaic width of about 60′. A third crystal, Cr-3, also grown from the vapor and about one-half the size of Cr-1, was used for certain measurements near T_N.

All of the experiments were performed on triple-axis spectrometers at the Brookhaven High Flux Beam Reactor. The incident neutron energy, monochromating crystals, and collimation were varied to optimize the configuration for a given measurement. The crystals were all mounted for scattering in the (100) reciprocal-lattice plane, either in a Displex refrigerator or variable-temperature cryostat for low-temperature work, and in a furnace for work at high temperatures.

In the longitudinally polarized spin-density-wave (LSDW) phase below 122 K, the magnetic satellite peak at $(0,0,1-\delta)$ disappears since the ordered moment is then along the neutron scattering vector. However, transverse fluctuations corresponding to precessional spin waves are observed near this point as shown in Fig. 3(a). As mentioned earlier, a single peak is observed in constant-E scans as the resolution ellipsoid passes through the very-high-velocity dispersion surface originating from the satellite position at $(0,0,1-\delta)$. These same spin waves can also be observed near the satellite reflection at $(0,1,\delta)$ as shown by the data in Fig. 3(b). If the excitations giving

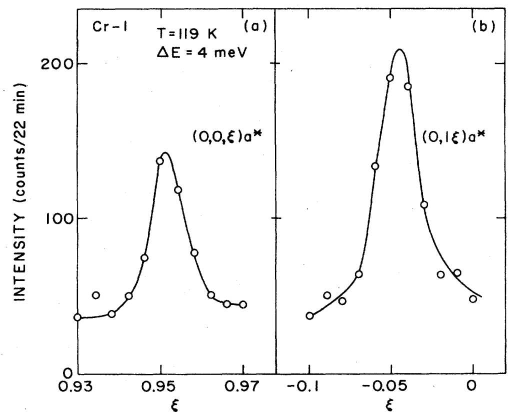

FIG. 3. Constant-ΔE scans through the spin waves at (a) $(0,0,1-\delta)$ and (b) $(0,1,\delta)$. The temperature is $T=119$ K, just below T_{sf}.

rise to this peak were strictly transversely polarized spin waves (transverse to **Q** and to the ordered moment), the intensity at $(0,1,\delta)$ would be expected to be approximately one-half of the intensity at $(0,0,1-\delta)$, because only the x component (normal to the scattering plane) of the transverse fluctuations of the magnetization are observable at this point in reciprocal space. In fact, nearly the reverse intensity ratio is observed. This means that the longitudinal susceptibility $\chi_{zz}(\mathbf{q},\omega)$, arising from fluctuations of the magnitude of the amplitude $\mathbf{M}_Q$ or perhaps the phase of the SDW, is larger (by more than a factor of 2) than the transverse susceptibility $\chi_{xx}(\mathbf{q},\omega)$ at this wave vector.

Just above the spin-flip temperature at $T=125$ K in the transversely polarized spin-density-wave (TSDW) phase, the spin-wave intensity at $(0,0,1-\delta)$ is observed to increase by nearly a factor of 2 above that seen just below T_{sf} as shown in Fig. 4(a). The same spin wave observed at $(0,1,\delta)$ is of nearly equal intensity to that observed at this same position below T_{sf} [Fig. 4(b)]. Since the intensities observed at these two positions in reciprocal space are roughly equal at 125 K, one might infer that the spin

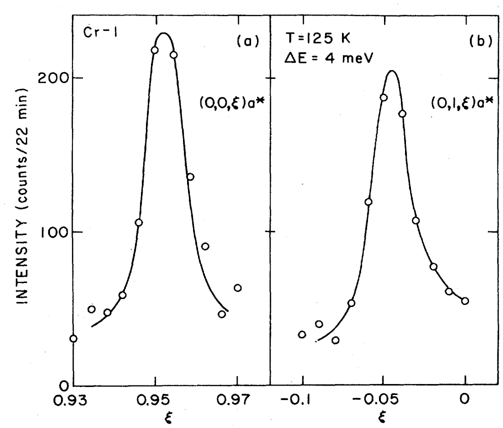

FIG. 4. Constant-ΔE scans through the spin waves at (a) $(0,0,1-\delta)$ and (b) $(0,1,\delta)$. The temperature is $T=125$ K, just above T_{sf}.

fluctuations corresponding to this excitation are isotropic at this temperature. However, since we now know that the longitudinal susceptibility is significant in the LSDW phase, there is no *a priori* reason to suppose that it will also not be important in the TSDW phase. Conclusions based on ideas of fluctuating (in angle) rigid, local moments will not correspond to the experimental facts in Cr. The recent observations of Burke *et al.*[12] of the energy dependence of the intensity ratio of the spin-wave peaks observed at $(0,0,1-\delta)$ and at $(0,1,\delta)$ in the TSDW phase show that these spin fluctuations become more anisotropic at low energies. In making these measurements we have carefully observed the relative intensities of nuclear Bragg reflections 90° apart, so as to eliminate anisotropic sample enclosure transmission effects alluded to in our earlier work.

We have now studied in some detail the overall evolution of the inelastic magnetic scattering cross section with temperature through the TSDW phase and far into the paramagnetic phase. The excitations which lead to the disappearance of the ordered state at T_N consist of two parts, which we have labeled "spin waves" and "commensurate-diffuse" scattering (see Fig. 2). The commensurate-diffuse scattering itself consists of two parts which we have called the "4-meV excitation" and the "quasielastic background" component. There is an indication of an additional excitation at 8 meV in some of our data. This has also been seen in the experiments of Burke *et al.*[12] The quasielastic background component increases very rapidly with decreasing energy transfer and also with increasing temperature as T approaches T_N as shown in Fig. 5. This scattering appears to be diverging at the Néel point. It is, in fact, increasing exponentially with T as shown by the plot on a log scale in Fig. 6. The intensity of the 4-meV excitation, taken separately by subtracting off the sloping quasielastic background scattering, increases more gradually with temperature, in rough accord with a Bose thermal factor. It is apparent that this

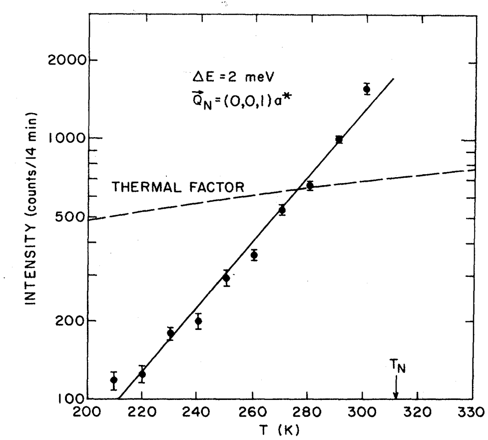

FIG. 6. Temperature dependence of the commensurate excitations at an energy transfer $\Delta E = 2$ meV plotted on a logarithmic scale, showing that this intensity increases exponentially with temperature. The variation of the thermal factor $(\langle n \rangle + 1)$ over this temperature range is shown for comparison.

commensurate-diffuse scattering is a characteristic of the TSDW phase; it is absent below T_{sf}.

We have carried out experiments at much higher-energy transfers, up to 42 meV. Representative data are shown in Fig. 7. There are some perplexing features of these data. First of all, the spin-wave peaks in the constant-E scans are barely visible (at these high energies) and are certainly not centered above the incommensurate Bragg satellite, but are substantially shifted inward toward the (0,0,1) point as the energy transfer becomes larger. This means that the dispersion surfaces originating at these incommensurate Bragg points are not simple conical surfaces, described by a single spin-wave velocity parameter. Secondly, the intensity in the immediate region around (0,0,1) is enhanced relative to the lower-energy scans. The overall trend of a wide assembly of this inelastic data is that as we move toward higher temperatures or toward

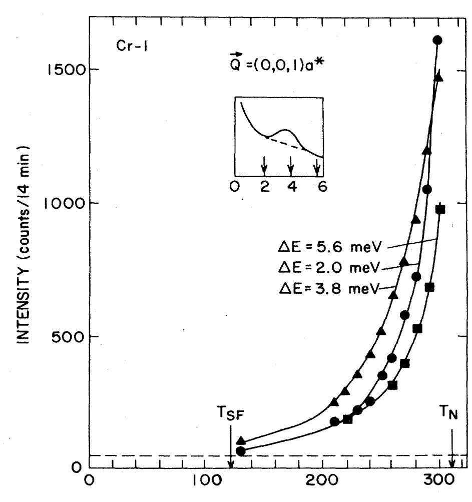

FIG. 5. Temperature dependence of the commensurate-diffuse modes at selected energy transfers.

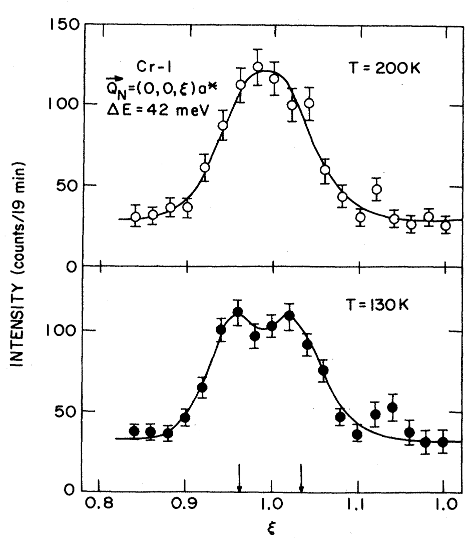

FIG. 7. Examples of constant-ΔE scans showing how the inelastic scattering evolves into a single peak centered at (0,0,1) as ΔE increases and also as the temperature is raised.

higher excitation energies, the scattering cross section evolves into a single diffuse, bell-shaped peak centered at (0,0,1).

Very-high-resolution experiments were performed to search for an energy gap in the spin-wave spectrum. Results of a constant-**Q** scan at (0,0,0.958) at 270 K are shown in Fig. 8. The incident neutron energy was 3.8 meV and the spectrometer energy resolution was about 20 μeV. Constant-E scans through this region show a peak at the Bragg satellite wave vector. Thus, there is a clear indication that excitations persist down to at least 50 μeV. This observation may also appear surprising if we were to think in terms of conventional spin-wave theory for localized moment antiferromagnetism in which a gap in the excitation spectrum is related to the product of the exchange interaction and the strength of the anisotropy field. From magnetic torque measurements[26] we know that there is a fourfold anisotropy in the **x**-**y** plane (normal to **Q**) and a very large anisotropy forcing the static SDW to be transversely polarized between T_{sf} and T_N. Since the spin-wave velocity is so high, an effective exchange parameter J should also be large. But, in spite of these considerations, there appears to be no significant energy gap.

We have searched for effects of a magnetic field (up to 60 kOe) on the excitation spectrum, with particular attention being given to the commensurate-diffuse modes. The magnetic field **H** was applied perpendicular to the scattering plane, and therefore perpendicular to the single **Q** direction. It is known from diffraction experiments[21,22] that the polarization of the SDW tends to rotate into a direction perpendicular to both **H** and **Q** under these conditions. This effect can be monitored by observing the decrease in the intensity of the (0,1,δ) satellite reflection as the field is increased. We show in Fig. 9 the results of constant-**Q** scans carried out at (0,0,1) at 270 K. For a field of 20 kOe the (0,1,δ) satellite intensity has decreased to about 15% of its zero-field value, indicating that the polarization of the SDW is largely along the **y** axis in the scattering plane (see Fig. 1). It is apparent that within experimental error there is no effect of the magnetic field on these excitations. Since the field-induced rotation of the polarization direction is basically reversible, and strongly temperature dependent, the lack of a measurable effect is surprising. It is possible that only the very-low-energy excitations (far below 1.5 meV) are effected by a magnetic field. The rapid increase in the quasielastic background scattering with decreasing energy transfer, referred to earlier, is apparent in the data of Fig. 9. The additional excitation at 8 meV is also indicated by this data.

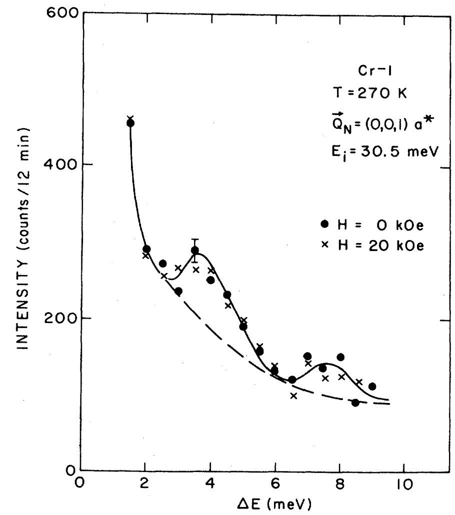

FIG. 9. Constant-**Q** scans at (0,0,1), searching for the effect of a magnetic field on the commensurate-diffuse scattering.

We turn our attention now to the disappearance of the ordered state at T_N and to the evolution of the magnetic scattering with temperature in the paramagnetic phase. Figure 10 shows the elastic intensity at the satellite position (0,0,1$-\delta$) at temperatures near the Néel point for Cr-2. It is evident that the transition is first order, but that some scattering persists above T_N. This scattering has been observed in a number of previous studies[27,28] and attributed to critical fluctuations. It is difficult to make this interpretation unambiguously because of the known influences of strain on the character of this transition. Small regions of the crystal may remain antiferromagnetic above T_N due to residual strain, and as the temperature is

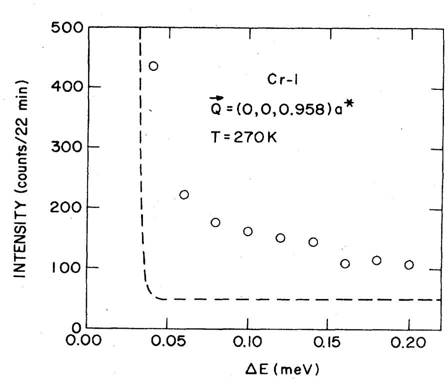

FIG. 8. High-resolution, constant-**Q** scan at $\mathbf{Q}_N=(0,0,1-\delta)a^*$. The dashed line is the instrumental background.

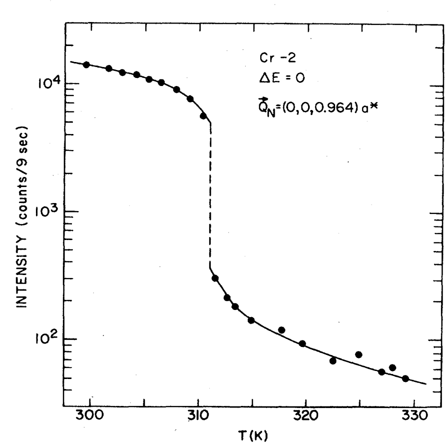

FIG. 10. Temperature dependence of the elastic scattering at the satellite position (0,0,1$-\delta$) in the vicinity of T_N.

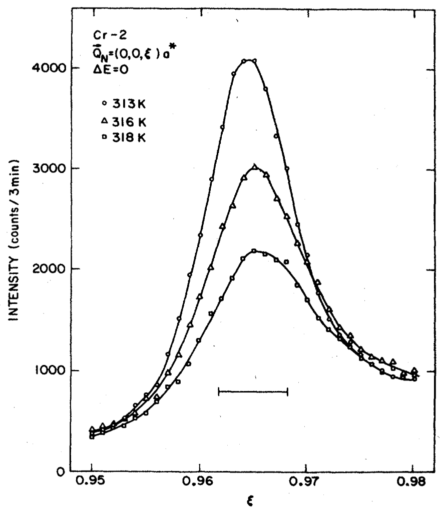

FIG. 11. Longitudinal elastic scans carried out on Cr-2 (strain-and-anneal crystal) for three temperatures just above T_N.

raised they decrease in size giving rise to a broadening in momentum space. In order to better understand the origin of this scattering we have made careful measurements on two different crystals near T_N. The two crystals were Cr-2, the large strain-and-anneal—grown crystal, and Cr-3, a small vapor-grown crystal. Figure 11 shows the results of longitudinal elastic scans through the $(0,0,1-\delta)$ satellite position at three temperatures just above T_N for Cr-2. A scan made on Cr-3 at 315 K under identical experimental conditions is shown in Fig. 12(a) and compared to the results of the 313-K data of Fig. 11, but replotted on a similar scale in Fig. 12(b). It is apparent that the shape of the two peaks are nearly identical. Since the size of Cr-3 is about one-eighth of Cr-2, it is noted that the intensities are also in good agreement. Because the

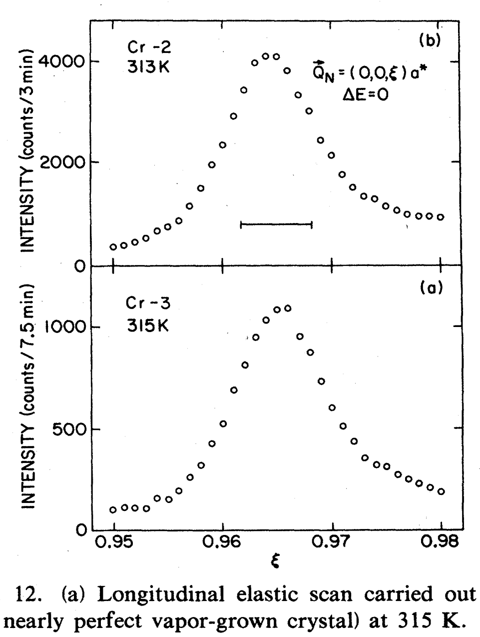

FIG. 12. (a) Longitudinal elastic scan carried out on Cr-3 (small, nearly perfect vapor-grown crystal) at 315 K. (b) Same scan for Cr-2 at 313 K shown in Fig. 11, but replotted on a scale to be compared to the data in (a).

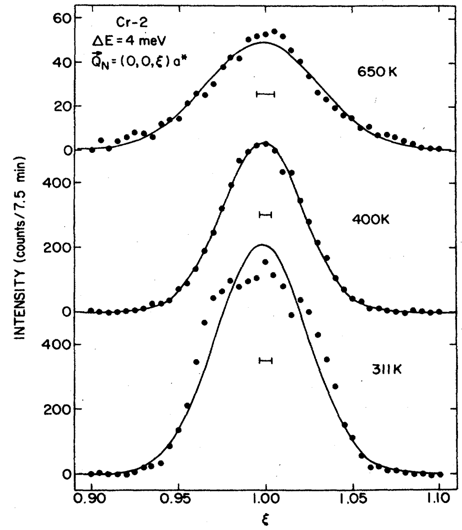

FIG. 13. Longitudinal scans along [001] at an energy transfer of 4 meV at three temperatures. The background has been subtracted. The solid lines are the results of fits to Gaussians. The lower scan at 311 K is just below T_N.

quality (and probably the residual strain) of these two crystals is so different, we conclude that the presence of this elastic scattering above T_N is an intrinsic property of chromium resulting from short-range ordering of the spins. From the width of the peak at 315 K we infer a coherent length of about 1000 Å at this temperature. These (elastic) peaks decrease in intensity and broaden as the temperature is increased, finally disappearing into the background at about 325 K.

As the temperature approaches the Néel point, the inelastic scattering is dominated by the commensurate-diffuse scattering, evolving into a single Gaussian-shaped peak in the paramagnetic phase. Examples of constant-energy scans at $\Delta E = 4$ meV are shown in Fig. 13. At 311 K, just below T_N, there remains only a slight hint of the incommensurate nature of the static SDW in this data. For this energy transfer, the intensity at (0,0,1) continues

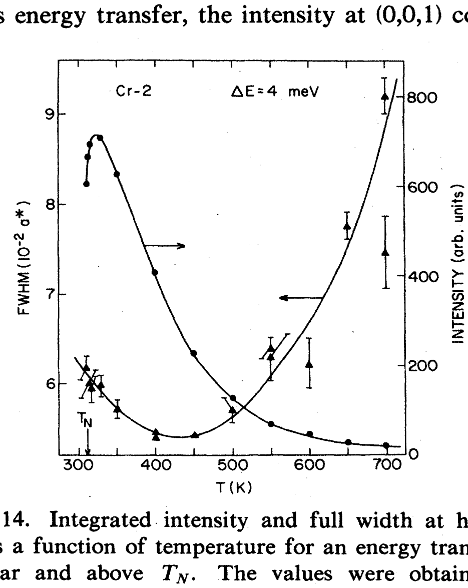

FIG. 14. Integrated intensity and full width at half maximum as a function of temperature for an energy transfer of 4 meV near and above T_N. The values were obtained from Gaussian fits to the data.

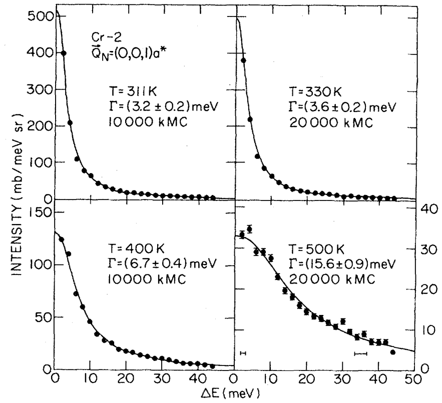

FIG. 15. Intensity as a function of energy transfer ΔE at $\mathbf{Q}=(0,0,1)a^*$ for four temperatures. The final neutron energy E_f was fixed at 30.5 meV. The data has been corrected for background and energy-dependent beam size effects. The solid lines are a resolution-broadened Lorentzian fit to the data. The monitor factor used for each set of data is given below the linewidth. See the Appendix for a discussion of the procedure used to convert the data to absolute units.

to increase for about 10 K above T_N and then decreases monotonically with increasing temperature as shown in Fig. 14. These data were fit to Gaussians centered at (0,0,1) convoluted with the instrumental resolution. The data cannot be fit to a Lorentzian at any temperature. The temperature dependence of the linewidths determined from the fits is also shown in Fig. 14. Above 350 K the Gaussian fits are excellent. The linewidth is not monotonic with temperature, but reaches a minimum at about 100 K above T_N. This conclusion is independent of the fitting procedure.

Although we have not followed the temperature dependence of the scattering at other energy transfers in such detail, the following general statements can be made on the basis of the data that we now have available: At all temperatures and energy transfers the scattering remains confined to a region close to (0,0,1) (and equivalent points in reciprocal space), dropping to near zero outside a sphere of radius $0.1a^*$. It appears to be isotropically disposed about (0,0,1). As the energy transfer is increased, the intensity peaks at temperatures further removed from T_N. The temperature dependence of the spectral distribution of magnetic intensity at $\mathbf{Q}_N=(0,0,1)a^*$ is shown in Fig. 15. The scattering extends over a progressively wider energy range as the temperature is raised. These data are

TABLE I. Energy dependence of the width of the paramagnetic scattering in momentum space. Values are full width at half maximum (FWHM) equal to 2.35σ in units of $0.01a^*$.

T (K)	$\Delta E=4$ meV	$\Delta E=10$ meV	$\Delta E=20$ meV
330	5.66±0.06	6.68±0.08	7.80±0.14
400	5.06±0.10	6.18±0.12	7.40±0.20
500	6.28±0.16	6.38±0.18	7.12±0.20

consistent with the observations reported by Booth *et al.*[28] and with the polarization analysis measurements of Ziebeck *et al.*[29] from which it was concluded that most of the magnetic scattering falls within their experimental energy window of about 50 meV. The solid lines in Fig. 15 are the result of fitting the data to a resolution-broadened Lorentzian. Corrections for background, the thermal population factor, and energy-dependent beam size effects were made in fitting the data. It is apparent that at temperatures somewhat removed from T_N in the paramagnetic phase the magnetic scattering cross section can be adequately described by the product of a Gaussian in momentum space centered at (0,0,1), and equivalent positions, and a Lorentzian in energy. That is, the dynamic structure factor takes on the remarkably simple form

$$S(\Delta\mathbf{q},\hbar\omega)=S_0(T)e^{-(\Delta q)^2/2\sigma^2}\frac{1}{(\hbar\omega)^2+\Gamma^2}\frac{\hbar\omega/kT}{1-e^{-\hbar\omega/kT}}\,, \tag{1}$$

where the last factor is the Bose thermal population number. It is clear from our data that σ is a slowly-varying function of temperature (see Fig. 14) and energy (see Table I), whereas Γ increases rapidly with temperature (see Fig. 15).

The data of Fig. 15 has been placed on an absolute scale (mb/meV sr atom) by normalizing to the integrated intensity of selected phonons. This allows us to relate the paramagnetic scattering to the wave-vector-dependent magnetic moment $\mathbf{m}(\Delta\mathbf{q})$ through the formula

$$f^2(\mathbf{q})\,|\,\mathbf{m}(\Delta\mathbf{q})\,|^2=\int S(\Delta\mathbf{q},\hbar\omega)d(\hbar\omega)\,, \tag{2}$$

where f is the magnetic form factor of a chromium atom, $\mathbf{m}$ is expressed in Bohr magnetons, and $\Delta\mathbf{q}$ has its origin at $(0,0,1)a^*$, as above. The values for $|\,m(\mathbf{0})\,|^2$ given in Table II are approximately a factor of 100 greater than those given by Ziebeck *et al.*,[29] in which the normalization was obtained using the incoherent scattering cross section. This discrepancy between our results and those

TABLE II. Measured paramagnetic cross section and magnetic moments. Error estimates shown are statistical and do not include systematic errors. These are discussed in the text.

T (K)	Measured cross section at $\Delta\mathbf{q}=\mathbf{0}$, $\hbar\omega=0$ [see Eq. (A5)] $KI(0)$ (mb/sr meV atom)	Resolution corrected cross section [see Eq. (A6)] $\frac{KI(0)}{\epsilon_v\epsilon_t}$ (mb/sr meV atom)	$\|\,m(\mathbf{0})\,\|^2$ (μ_B^2)	μ_{eff} (μ_B)
330	494±78	1428±244	698±158	0.28±0.03
400	138±22	464±87	422±104	0.18±0.02
500	33±5	84±16	178±45	0.16±0.02

of Ref. 29 may result from an improper treatment of the effects of the shape and orientation of the resolution function in the polarized beam studies. Our measurements of the ratio of the incoherent scattering cross section to the phonon cross section is in agreement with other published data. The effective moment per atom, $\mu_{\rm eff}$, in the paramagnetic state of chromium is of considerable, long-standing importance. The formula for $\mathbf{m}(\Delta\mathbf{q})$ given by Eq. (2) can be regarded as a definition, but the calculation of $\mu_{\rm eff}$ from the data requires a model and certain assumptions (or additional information) regarding the scattering cross section and the instrumental resolution. The values for $\mu_{\rm eff}$ given in Table II were obtained by the procedure outlined in the Appendix. The rms magnetic moment per atom in the ordered state is $0.43\mu_B$ and the discontinuity in the ordered moment at T_N is approximately $0.12\mu_B$.[20] Thus, a fair fraction of moment remains at temperatures just above T_N.

It is interesting and perhaps important to note that magnetic correlations in the paramagnetic state extend over 11—14 unit cells to very high temperatures—a distance which is nearly the same as the spacing between the nodes of the SDW in the ordered state. Experiments on the spatial correlations in commensurate *Cr*Mn alloys are underway to investigate the relationship of these long correlation ranges to commensurability.

IV. CONCLUSIONS

The antiferromagnetism in chromium continues to provide us with challenging surprises and puzzles. There are few aspects of the excitation spectrum revealed by the experiments described in this paper, and also in other recent studies, that were predicted by, or can now be interpreted by any theory. The energy and temperature dependence of the inelastic scattering below T_N is difficult to describe in any simple way, but it clearly involves much more than simple spin waves originating at the incommensurate magnetic Bragg reflections. The recent, higher-resolution experiments of Burke *et al.*[12] revealing additional structure of the commensurate-diffuse scattering and its suggested connection with the longitudinal (0,0,1) acoustic phonons need further study. The fact that this scattering is only observed between the magnetic satellites and not at wave vectors smaller than $(0,0,1-\delta)$ and greater than $(0,0,1+\delta)$ contradicts this interpretation.

The disappearance of the long-range, incommensurate ordered phase at T_N seems to be dominated by the commensurate-diffuse modes. It is therefore important to study the temperature dependence of these modes at considerably lower energies in the vicinity of T_N. In the paramagnetic phase the scattering remains highly confined to the region surrounding the (0,0,1), and at no temperature is there any evidence for ordinary paramagnetic scattering resulting from single $3d$ magnetic atoms. The paramagnetism appears to be a highly correlated regime with spatial coherence extending over 11 to 14 bcc unit cells in the temperature range investigated.

It is apparent from our limited data below $T_{\rm sf}$ that the longitudinal fluctuations of the static SDW are very important. Essentially nothing is known, either experimentally or theoretically, about the phase fluctuations of a SDW ground state.[30] These modes may contribute to the longitudinal susceptibility. There appears to be several possible modes of excitation of the static SDW in chromium.

(1) *Ordinary spin waves* which can be viewed classically as precessional modes of the $3d$ atomic moments.

(2) *Amplitude modes* for which the magnitude of the amplitude $\mathbf{M}_Q$ of the SDW fluctuates.

(3) *Phason modes* for which the phase of the SDW as a whole fluctuates, or for which the relative phase of the spin-up and spin-down electron densities fluctuate. This relative phase fluctuation would give rise to dynamic charge-density waves.

The relative importance of these three types of excitations in chromium is not known at all at the present time. There is no reason to suppose that these various modes are independent, or even propagating. Future progress will depend partly upon new theoretical insights. It is likely that a more fundamental theory of the magnetic excitations of the SDW in chromium observed in this study will lead to a better general understanding of magnetism in all metals.

ACKNOWLEDGMENTS

Work at Brookhaven National Laboratory was supported by the Division of Materials Sciences, U.S. Department of Energy, under Contract No. DE-AC02-76CH00016. One of us (S.A.W.) would like to acknowledge support of the National Science Foundation through Grant No. DMR-82-00350.

APPENDIX: NORMALIZATION OF THE PARAMAGNETIC SCATTERING AND THE CALCULATION OF THE EFFECTIVE MOMENT PER Cr ATOM, $\mu_{\rm eff}$

In order that the steps and assumptions used in calculating $\mu_{\rm eff}$ can be easily traced, we give our method and logic here in some detail. The scattering intensity is normalized to the energy-integrated phonon creation cross section obtained for fixed $(1/v)$ monitor counts, and fixed final energy, namely[31]

$$\left[\frac{d\sigma}{d\Omega}\right]_{\rm phonon}=BN\frac{b^2Q_N^2\cos^2\beta}{M\hbar\omega}\langle n(\hbar\omega)+1\rangle e^{-2W}\,, \tag{A1}$$

where $B=2.09$ b/sr, N is the number of atoms in the crystal, b^2 is the square of the coherent scattering length per atom in b, $\mathbf{Q}_N$ is the neutron scattering vector in Å^{-1}, β is the angle between the scattering vector and the phonon polarization vector, M is the atom mass in amu, and $\hbar\omega$ is the phonon energy in meV. For Cr, $M=51.996$, $b=0.3635\times10^{-12}$ cm. We show in Fig. 16 the (011) TA phonon measured at $\mathbf{Q}_N=(0,1.1,0.9)a^*$ at $T=400$ K. For this phonon, $\hbar\omega=9.07$ meV, and Eq. (A1) gives

$$\left[\frac{d\sigma}{d\Omega}\right]_{\rm phonon}=24.1\ \text{mb/sr atom}\,, \tag{A2}$$

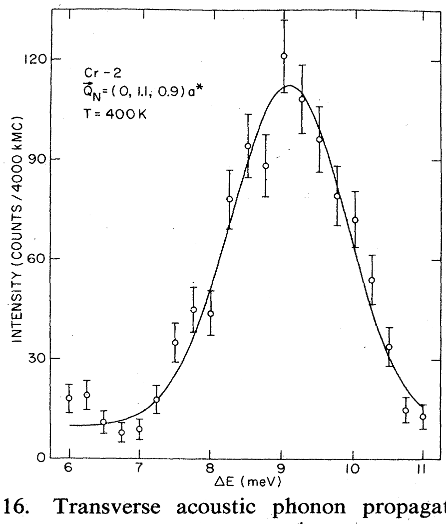

FIG. 16. Transverse acoustic phonon propagating along $[0\bar{1}1]$, measured at $\mathbf{Q}_N=(0,1.1,0.9)a^*$ at $T=400$ K, with the same spectrometer configuration as the data shown in Fig. 15.

where we have set the Debye-Waller factor $e^{-2W}\approx 1$. The integrated intensity of this phonon is

$$I_{\text{phonon}}=(207 \text{ counts meV})/(4000 \text{ kMC}) \ . \tag{A3}$$

where kMC stands for thousands of monitor counts.

Thus, the instrumental conversion factor K is obtained by dividing (A2) by (A3):

$$K=464\frac{\text{mb kMC}}{\text{meV sr atom count}} \ . \tag{A4}$$

This is the factor used to produce Fig. 15.

The normalization of the paramagnetic scattering to an integrated phonon cross section only strictly works if the magnetic scattering is broad in $\hbar\omega$ and $\Delta\mathbf{q}$ compared to the resolution ellipsoid. This is not quite the case for our experiment; however, we can estimate a correction for this effect as shown below. We denote $I(0)$ the measured magnetic scattering counting rate (counts/kMC), extrapolated to $\Delta\mathbf{q}=\mathbf{0}$ and $\hbar\omega=0$; then

$$KI(0)=\frac{1}{N}\left[\frac{d^2\sigma_{\text{mag}}}{d\Omega\, dE'}(\Delta\mathbf{q}=\mathbf{0},\hbar\omega=0)\right]_{\text{measured}} \tag{A5}$$

is the measured magnetic scattering cross section in mb/sr meV atom. Values for this cross section are tabulated in Table II for three temperatures. The energy resolution and the longitudinal $\mathbf{q}$ resolution are sufficiently sharp at these temperatures to neglect this effect on the measured cross section. However, the transverse (t) and vertical (v) $\mathbf{q}$ resolutions are not quite sharp enough. Let σ_v be the Gaussian width of the vertical resolution, and σ_t the transverse resolution width. In our experiment $2.35\sigma_v=0.069a^*$ and $2.35\sigma_t=0.087a^*$. We denote

$$\epsilon_v\equiv\frac{\sigma}{(\sigma_v^2+\sigma^2)^{1/2}} \text{ and } \epsilon_t\equiv\frac{\sigma}{(\sigma_t^2+\sigma^2)^{1/2}} \ , \tag{A6}$$

where σ is the Gaussian width of the paramagnetic scattering cross section in Eq. (1). We must increase the measured cross section in Eq. (A5) by $1/\epsilon_v\epsilon_t$ in order to compare it with a theoretical calculation of $(d^2\sigma/d\Omega\, dE')$ evaluated at $\Delta\mathbf{q}=\mathbf{0}$, $\hbar\omega=0$. This resolution correction is approximately a factor of 3, and the results are given in the second column of Table II.

The paramagnetic scattering cross section is related to the dynamic structure factor by

$$\left\langle\frac{d^2\sigma}{d\Omega\, dE'}\right\rangle_\alpha=\frac{2}{3}\left[\frac{\gamma r_0}{2}\right]^2\frac{k'}{k}NS(\Delta\mathbf{q},\hbar\omega) \ , \tag{A7}$$

where $\gamma=1.913$ and $r_0=e^2/mc^2=0.282\times10^{-12}$ cm. The angular brackets $\langle\ \rangle_\alpha$ denote that an isotropic (cubic) average over spin directions, specified by α, has been assumed. This accounts for the factor $\frac{2}{3}$. The numerical constants in Eq. (A7) are consistent with our definition of $\mathbf{m}(\Delta\mathbf{q})$ in terms of $S(\Delta\mathbf{q},\hbar\omega)$ given by Eq. (2). The wave-vector-dependent magnetic moment is given explicitly in terms of the Fourier transform $\mathbf{M}(\mathbf{q})$ of the magnetization $\widetilde{M}(\mathbf{r})$ by

$$\begin{aligned} f^2(q)\,|\,m(\mathbf{q})\,|^2&=\frac{|\,M(\mathbf{q})\,|^2}{N\mu_B^2}\\ &=\frac{V}{N\mu_B^2}\int_V\langle\widetilde{M}(0)\cdot\widetilde{M}(\mathbf{r})\rangle e^{i\mathbf{q}\cdot\mathbf{r}}d^3r \ , \end{aligned} \tag{A8}$$

where V is the crystal volume.

Experimentally we have found that the scattering cross section is Lorentzian in $\hbar\omega$ (after dividing out the thermal factor), and Gaussian in $\Delta\mathbf{q}$. Thus, we write with proper spectral normalization

$$\begin{aligned} S(\Delta\mathbf{q},\hbar\omega)=&f^2(\mathbf{Q}_N)\,|\,m(0)\,|^2e^{-(\Delta q)^2/2\sigma^2}\frac{1}{\pi}\\ &\times\frac{\Gamma}{\Gamma^2+(\hbar\omega)^2}\frac{\hbar\omega/kT}{1-e^{-\hbar\omega/kT}} \ . \end{aligned} \tag{A9}$$

At $\Delta\mathbf{q}=\mathbf{0}$ and $\hbar\omega=0$ we have

$$S(0,0)=f^2\,|\,m(\mathbf{0})\,|^2\frac{1}{\pi\Gamma} \ , \tag{A10}$$

and at (0,0,1), $f=0.69$, so that using (A7) we find

$$\frac{1}{N}\left\langle\frac{d^2\sigma}{d\Omega\, dE'}\right\rangle_\alpha=\frac{7.36}{\Gamma}\,|\,m(\mathbf{0})\,|^2 \text{ mb/sr meV atom} \ . \tag{A11}$$

Here Γ is in meV (see Fig. 15), $|\,m(\mathbf{0})\,|^2$ is in Bohr magnetons squared. With use of this relation, the results for $|\,m(\mathbf{0})\,|^2$ given in Table II are obtained.

The effective moment per atom μ_{eff} is obtained by integrating the magnetization $\widetilde{M}(\mathbf{r})$ surrounding each atom (over the atom volume equal to $a^3/2$) and averaging over the crystal. Using Eq. (A8) it is straightforward to show that

$$\mu_{\text{eff}}^2=\tfrac{1}{2}(a/2\pi)^3\int|\,m(\Delta\mathbf{q})\,|^2d^3\Delta\mathbf{q} \ , \tag{A12}$$

or

$$\mu_{\text{eff}}^2=\tfrac{1}{2}(a/\sqrt{2\pi})^3\sigma^3\,|\,m(\mathbf{0})\,|^2 \ . \tag{A13}$$

The values for μ_{eff} in Table II were obtained using this formula, in which the $\Delta E=4$ meV values of the width parameter σ, given in Table I, were used. This is an approximation since σ is a function of energy, and a weighted average over the spectral intensity should really be carried out. However, more detailed data is required to substantially improve the estimate of $\mu_{\rm eff}$ made here. It is also implicit in our procedure here that the energy width Γ is a function only of temperature, and not of the wave-vector distance $\Delta\mathbf{q}$ away from the (0,0,1) point. The use of a Lorentzian in Eq. (A9) also leads to an overestimate of $\mu_{\rm eff}$ since the scattering must fall off faster than this at large energy transfers. These assumptions and approximations are reasonable and contribute to an estimated uncertainty in the values of $\mu_{\rm eff}$ in Table II of no more than about 20%.

*Present address: Physics Department, West Virginia University, P.O. Box 6023, Morgantown, WV 26506-6023.

†On leave from Department of Physics and Astronomy, University of Missouri—Columbia, Columbia, MO 65211.

[1]L. M. Corliss, J. M. Hastings, and R. Weiss, Phys. Rev. Lett. **3**, 211 (1959).

[2]V. N. Bykov, V. S. Golovkin, N. V. Ageev, V. A. Levdik, and S. I. Vinogradov, Dokl. Akad. Nauk SSSR **128**, 1153 (1959) [Sov. Phys.—Dokl. **4**, 1070 (1960)].

[3]A. W. Overhauser, Phys. Rev. **128**, 1437 (1962).

[4]W. M. Lomer, Proc. Phys. Soc. London **86**, 489 (1962).

[5]For a discussion of the Fermi-surface topology, see R. Reifenbergen, F. W. Holroyd, and E. Fawcett, J. Low Temp. Phys. **38**, 421 (1980).

[6]For a review of these models, see E. W. Fenton and G. R. Leavens, J. Phys. F **10**, 1853 (1980), and references therein.

[7]C. R. Fincher, Jr., G. Shirane, and S. A. Werner, Phys. Rev. Lett. **43**, 1441 (1979).

[8]K. Mikke and J. Jankowski, J. Magn. Magn. Mater. **14**, 280 (1979); J. Phys. F **10**, L159 (1980).

[9]C. R. Fincher, Jr., G. Shirane, and S. A. Werner, Phys. Rev. B **24**, 1312 (1981). (This is paper I in the present series.)

[10]K. R. A. Ziebeck and J. G. Booth, J. Phys. F **9**, 2424 (1979).

[11]S. A. Werner, G. Shirane, C. R. Fincher, Jr., and B. H. Grier, in *Neutron Scattering—1981,* edited by John Faber Jr. (AIP, New York, 1982), p. 269.

[12]S. K. Burke, W. G. Stirling, and K. R. A. Ziebeck, Phys. Rev. Lett. **51**, 494 (1983).

[13]P. A. Fedders and P. C. Margin, Phys. Rev. **143**, 245 (1966).

[14]S. H. Liu, J. Magn. Magn. Mater. **22**, 93 (1980).

[15]H. Sato and K. Maki, Int. J. Magn. **6**, 183 (1974).

[16]J. Als-Nielsen, J. D. Axe, and G. Shirane, J. Appl. Phys. **42**, 1666 (1971).

[17]S. K. Sinha, S. H. Liu, L. D. Muhlestein, and N. Wakabayashi, Phys. Rev. Lett. **23**, 311 (1969); S. K. Sinha, G. R. Kline, C. Stassis, and N. Chesser, Phys. Rev. B **15**, 1415 (1977).

[18]T. Wolfram and E. Ellialtioglu, Phys. Rev. Lett. **44**, 1295 (1980).

[19]A. Arrott, S. A. Werner, and H. Kendrick, Phys. Rev. Lett. **14**, 321 (1965).

[20]S. A. Werner, A. Arrott, and H. Kendrick, Phys. Rev. **155**, 528 (1967).

[21]S. A. Werner, A. Arrott, and M. Atoji, J. Appl. Phys. **39**, 671 (1968).

[22]S. A. Werner, A. Arrott, and M. Atoji, J. Appl. Phys. **40**, 1447 (1968).

[23]R. H. Beumont, H. Chichara, and J. A. Morrison, Philos. Mag. **5**, 188 (1960).

[24]M. K. Wilkinson, E. O. Wollan, W. C. Koehler, and J. W. Cable, Phys. Rev. **127**, 2080 (1962).

[25]G. E. Bacon and N. Cowlam, J. Phys. C **2**, 238 (1969).

[26]M. O. Steinitz, L. H. Schwartz, J. A. Marcus, E. Fawcett, and W. A. Reed, Phys. Rev. Lett. **23**, 979 (1969).

[27]H. B. Moller, K. Blinowski, A. R. Mackintosh, and T. Brun, Solid State Commun. **2**, 109 (1964).

[28]J. G. Booth, K. R. A. Ziebeck, and C. Escribe, J. Magn. Magn. Mater. **14**, 135 (1979).

[29]K. R. A. Ziebeck, J. G. Booth, P. J. Brown, H. Capellmann, and J. A. C. Bland, Z. Phys. B **48**, 233 (1982).

[30]Phase fluctuations of charge-density waves CDW's leading to elementary excitations called phasons have attracted considerable attention starting with their theoretical prediction by A. W. Overhauser, Phys. Rev. B **3**, 3173 (1971).

[31]See, for example, O. Steinsvoll, C. F. Majkrzak, G. Shirane, and J. Wicksted, Phys. Rev. B **30**, 2377 (1984).